Osmane, Adnane; Wilson, Lynn B.; Blum, Lauren; Pulkkinen, Tuija I.

On the connection between microbursts and nonlinear electronic structures in planetary radiation belts

Published in:
The Astrophysical Journal

DOI:
10.3847/0004-637X/816/2/51

Published: 10/01/2016

Document Version
Publisher's PDF, also known as Version of record

Please cite the original version:
Osmane, A., Wilson, L. B., Blum, L., & Pulkkinen, T. I. (2016). On the connection between microbursts and nonlinear electronic structures in planetary radiation belts. *The Astrophysical Journal*, *816*(2), Article 51. https://doi.org/10.3847/0004-637X/816/2/51

The Astrophysical Journal, 816:51 (10pp), 2016 January 10 doi:10.3847/0004-637X/816/2/51

ON THE CONNECTION BETWEEN MICROBURSTS AND NONLINEAR ELECTRONIC STRUCTURES IN PLANETARY RADIATION BELTS

Adnane Osmane[1], Lynn B. Wilson III[2], Lauren Blum[3], and Tuija I. Pulkkinen[1]
[1] Department of Radio Science, Aalto University, FI-02150, Finland; adnane.osmane@aalto.fi, tuija.pulkkinen@aalto.fi
[2] NASA Goddard Space Flight Center, Greenbelt, MD, USA; lynn.b.Wilsoniii@gmail.com
[3] Space Sciences Laboratory, Berkeley, CA, USA; lwblum@ssl.berkeley.edu
Received 2015 July 15; accepted 2015 November 11; published 2016 January 5

ABSTRACT

Using a dynamical-system approach, we have investigated the efficiency of large-amplitude whistler waves for causing microburst precipitation in planetary radiation belts by modeling the microburst energy and particle fluxes produced as a result of nonlinear wave–particle interactions. We show that wave parameters, consistent with large-amplitude oblique whistlers, can commonly generate microbursts of electrons with hundreds of keV-energies as a result of Landau trapping. Relativistic microbursts (>1 MeV) can also be generated by a similar mechanism, but require waves with large propagation angles $\theta_{kB} > 50^\circ$ and phase-speeds $v_\Phi \geqslant c/9$. Using our result for precipitating density and energy fluxes, we argue that holes in the distribution function of electrons near the magnetic mirror point can result in the generation of double layers and electron solitary holes consistent in scales (of the order of Debye lengths) to nonlinear structures observed in the radiation belts by the Van Allen Probes. Our results indicate a relationship between nonlinear electrostatic and electromagnetic structures in the dynamics of planetary radiation belts and their role in the cyclical production of energetic electrons ($E \geqslant 100$ keV) on kinetic timescales, which is much faster than previously inferred.

Key words: acceleration of particles – Earth – plasmas – relativistic processes – solar–terrestrial relations – waves

1. INTRODUCTION

The last 10 years have shown what could potentially be described as a paradigm shift in our understanding of planetary radiation belts' properties and dynamics. The observation that wave–particle interactions might dominate the transport properties of electrons (Green & Kivelson 2004; Chen et al. 2007; Reeves et al. 2013), followed a few years later by the discovery of large-amplitude ($\delta E \geqslant 100$ mV m^{-1}), obliquely propagating $\theta_{kB} > 40$, quasi-monochromatic whistlers (LAWs) observed in the lower band frequency range (Cattell et al. 2008, 2012; Cully et al. 2008; Kellogg et al. 2010, 2011; Breneman et al. 2011, 2012; Kersten et al. 2011; Wilson et al. 2011; Agapitov et al. 2014; Artemyev et al. 2015), and the more recent observations of nonlinear electronic structures (Kellogg et al. 2010; Mozer et al. 2013, 2014; Malaspina et al. 2014), have irremediably altered our comprehension of radiation belts. For instance, the discovery of large-amplitude whistlers with Poynting flux over four orders of magnitude above previous estimates (Wilson et al. 2011) raises fundamental questions as to the validity of quasi-linear theory (e.g., Diamond et al. 2010) as a means to quantify wave–particle interactions and transport coefficients (Thorne et al. 2013). The realization that electric fields that are intermittent but large, parallel to the mean magnetic field, are commonly observed in the radiation belts, has led to a growing number of studies of nonlinear wave–particle interactions applied to the Earth's radiation belts (Bortnik et al. 2008; Tao & Bortnik 2010; Yoon 2011; Artemyev et al. 2012, 2014a, 2014b, 2014c; Osmane & Hamza 2012b, 2014; Yoon et al. 2013, 2014; Osmane & Pulkkinen 2014; Woodroffe & Streltsov 2014; Drake et al. 2015).

Despite the inherent difficulty to observe and quantify the impact of LAWs due to their bursty nature and the necessity for high time resolution instruments, there is already observational evidence of their possible role in the generation of microburst events (Kersten et al. 2011). Rapid, millisecond-long bursts of electron precipitation, termed microbursts, have been measured by numerous missions at energies ranging from keV (Anderson & Milton 1964; Parks 1978) up to MeV, or relativistic energies (Imhof et al. 1992; Nakamura et al. 1995; Blake et al. 1996). Though the correlation between chorus waves and electron energization in the radiation belts is not recent (Lorentzen et al. 2001; Summers & Omura 2007; Hikishima et al. 2010; Lakhina et al. 2010; Tsurutani et al. 2013), new theoretical studies demonstrate that LAWs could be particularly efficient, energizing electrons by 10–80 keV and pitch-angle scattering ($\Delta\alpha \sim 1^\circ$–$7^\circ$) electrons on timescales consistent with microburst events (Artemyev et al. 2012, 2014a; Osmane & Hamza 2012b, 2014). For electrons with kinetic energies of tens of keV, interacting with typical LAWs, the energy gain of factors of two was associated with Landau trapped orbits (Artemyev et al. 2012; Osmane & Hamza 2014).

In this report, we quantify particle and energy precipitation fluxes generated by LAWs across a wide range of wave properties. Wave parameters (phase-speeds v_Φ and propagation angles θ_{kB}) are not limited to the cold plasma dispersion approximation. Recent observations by Kellogg et al. (2010) and Mozer et al. (2013) in the radiation belts and Kellogg et al. (2011) in the magnetosphere show that the nonlinear electron structures and waveforms are not always consistent with the cold plasma dispersion relation, which explains the need for widening the scope of the theoretical treatment herein. Consequently, our study also quantifies energy and particle fluxes generated by whistlers with $v_\Phi \geqslant c/6$ and $\theta_{kB} \geqslant 50^\circ$, that is, parameters inconsistent with the cold plasma dispersion relation. This extension beyond the cold plasma dispersion limits is useful as it shows the transition between keV and MeV microbursts. The range of wave amplitude $\delta B/B_0$ is also chosen between 0.1% and 10%. This range of wave amplitude is based on the statistical study of Wilson et al. (2011), in which, even though the bulk of the amplitudes were measured between

0.1% and 1%, whistlers with amplitudes of 10% were also observed. Hence, our study is specifically designed to quantify the effect of a wide range of wave properties (amplitude, frequency, and refractive index) on the precipitating fluxes. The investigated hypothesis is that despite the short-timescale interaction with LAWs, pitch-angle scattering during the trapping of Landau-resonant electrons might be sufficiently strong to result in 10–100 ms microbursts with classical and perhaps relativistic levels. Following our description of precipitation fluxes for various wave parameters, we use our results to argue that due to electron losses, holes in the distribution function can result in the generation of double layers and electron solitary holes on timescales consistent with the observation of Mozer et al. (2013, 2014), Malaspina et al. (2014), and the recent numerical investigation of Drake et al. (2015).

2. MOTIVATION

2.1. Landau Trapping by LAWs

The results of Osmane & Hamza (2012b, 2014) and Artemyev et al. (2012, 2014a) are the motivation of the current study and can be summarized by using a simple kinematic argument. Landau-resonant electrons near the equatorial plane can be trapped in the potential of the parallel electric field for a time $T \sim \cos(\theta_{kB}) s_{\rm trap}/v_\phi$, for the propagation angle θ_{kB}, the phase-speed v_ϕ, and the distance along the field line $s_{\rm trap}$. The trapping in the potential of the parallel electric field is terminated as a result of the preservation of the first adiabatic invariant $\mu = p_\perp^2/2mB$, whenever the electric force is of the same order and opposite to the magnitude as the magnetic mirror force, i.e., $q\delta E_\parallel \sim \frac{\mu}{\gamma}\nabla_\parallel B$, where the first invariant μ is written in terms of the perpendicular momentum $p_\perp = m\gamma v_\perp$, Lorentz factor γ and rest mass m. Assuming an inhomogeneous magnetic field $B(s) = B_0\left(1 + \frac{9 s_\parallel^2}{2L^2R_{\rm E}^2}\right)$ for an L-shell L, the Earth's radius $R_{\rm E}$ and the distance along the field line $s_\parallel$, it is straightforward to show that

$$s_{\rm trap} \sim \frac{4\pi}{9}\frac{\delta_1}{\nu}\frac{\gamma}{\gamma^2-1}\frac{L^2R_{\rm E}^2}{\lambda}\left(n^2\sin(\alpha)^2\right)^{-1}, \quad (1)$$

for the ratio of the wave amplitude to the background magnetic field $\delta_1 = \delta B/B_0$, the wave frequency to the gyro-frequency in the equatorial plane $\nu = \omega/\Omega_0$, the wavelength $\lambda = 2\pi/k$, pitch angle α, and refractive index $n = ck/\omega$. For the cold plasma approximation, the whistler dispersion relation can be approximated to

$$n^2 = \frac{\omega_{\rm pe}^2/\Omega_0^2}{\nu\left(\cos(\theta_{kB}) - \nu\right)}, \quad (2)$$

for the plasma frequency $\omega_{\rm pe}$ whenever $\omega_{\rm pe} \gg \Omega_0 = eB_0/mc$ and $\omega_{\rm pe} \gg \omega$.

Using the above approximations for the trapping length, we can plot the timescale of interaction Δ of an electron near the equatorial plane as a function of wave properties. In panel (a) of Figure 1, an estimation of the timescale of interaction for an electron with a large-amplitude whistler sub-element as a function of the Lorentz factor γ and the propagation angle θ is plotted. The interaction timescale is typically of the order of $\omega\Delta \sim 10$, i.e., $\Delta \sim 10$ ms for a whistler wave of frequency $\omega = 3$ kHz. In panel (b), we integrated the full set of equations of motion for a test-electron (Osmane & Hamza 2014, or see Section 2 below) to demonstrate the validity of this estimate for a typical orbit trapped by the LAWs in the equatorial plane. Despite the short timescale for the resonant interaction, relativistic electrons can gain a large amount of energy in the parallel direction and experience a significant reduction of their pitch angle while interacting with the parallel electric field (Artemyev et al. 2012, 2014a; Osmane & Hamza 2012b, 2014). The change in pitch angle during a single interaction occurs on timescales of the order of 10 ms, and is observed to be significant with $\Delta\alpha \sim 4°$–$5°$, bringing the electron in or near the loss cone. The short timescales involved result in the wave–particle interaction with a single sub-element of the LAW wave packet. Following the interaction with LAW sub-element, the electron reaches larger magnetic field regions, and its dynamics become dominated by the magnetic field mirror force. In panel (c), we plot the cold plasma dispersion relation as a function of propagation angle and wave frequency $\nu = \omega/\Omega_0$. We note that the cold plasma dispersion relation indicates that large propagation angles are associated with large refractive indices/small phase-velocities, and vice-versa.

3. METHODOLOGY

3.1. Nonlinear Wave–Particle Interaction

We use the dynamical-system approach developed in previous studies[4] by Osmane & Hamza (2012a, 2012b, 2014) to compute test-electron orbits with initial pitch angle α_0 and energy $m\gamma_0 c^2$. Each electron orbit is initially located at the equatorial plane with a divergence-free and inhomogeneous magnetic field written as $\boldsymbol{B}_0 = -yB_0 g'(z)\hat{y} + B_0 g(z)\hat{z}$, for the function $g(z) = 1 + \frac{z^2}{L^2R_{\rm E}^2}$. The whistler wave propagates obliquely to the background magnetic field as indicated by the angle θ_{kB} defined by $\cos(\theta_{kB}) = \boldsymbol{k}\cdot\boldsymbol{B}_0$ and with constant amplitude. The magnetic field fluctuations are written as $\delta B_{x,y} \propto \cos(kz - \omega t)$. The transverse electric field is given by Faraday's equation $\boldsymbol{k} \times \boldsymbol{\delta E}_T(k,\omega) = \omega/c\,\boldsymbol{\delta B}(k,\omega)$ and the longitudinal component is set as 40% of the transverse component, i.e., $\delta E_k = 0.4\delta E_T$.[5] The orbits are computed from the relativistic Lorentz Equation (Osmane & Hamza 2012a, 2012b, 2014) for a time interval of $\omega T = 20$, for a wave frequency ω typically of the order of 3 kHz, or when normalized, written as $\nu = \omega/\Omega_0$ with values ranging between [0.1, 0.5]. Following previous work, we write the other relevant parameters for our problem as $\delta_1 = \delta B/B_0$ for the relative wave amplitude and $n = c/v_\phi$ for the refractive index. We then compute the change in pitch angle during the Landau-resonant interaction, typically of 10–20 ms for a wave frequency $\omega = 0.1\Omega_e$, then determine whether the particles can enter the loss cone after a single interaction with the LAW. Even though the wave model we use is limited in scope, it is sufficient for our purpose. Large-amplitude whistlers typically have sub-elements with 30 ms duration (Santolik et al. 2001) and the wave–particle interaction timescale is of the order of 1–10 ms.

[4] We hereafter summarize the main properties of the dynamical system. Readers can find a detailed description of the dynamical system in the above references.

[5] It should be pointed out that the inclusion of a transverse component is not necessary and one can follow the approach of Artemyev et al. (2012, 2014) by including purely electrostatic whistler waves. The only two necessary physical requirements are for a parallel electric field, hence the obliquity, and sufficiently large-amplitude for physical trapping in the potential of the wave.

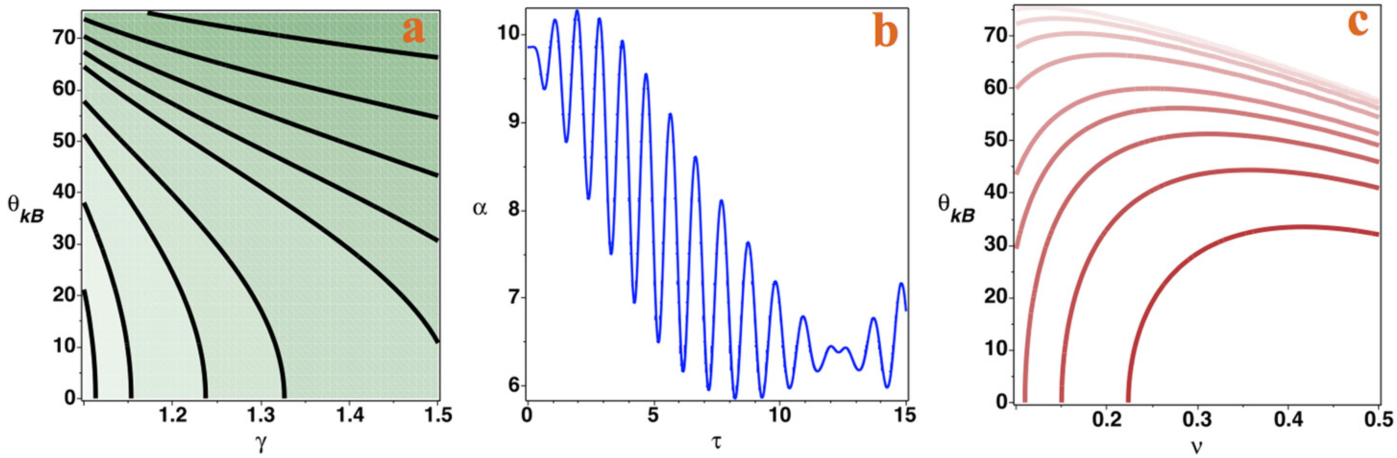

Figure 1. Estimation of the timescale of interaction Δ for an electron with a large-amplitude whistler sub-element as a function of the Lorentz factor γ and the propagation angle θ on panel (a). The contours are drawn, starting from the upper right corner, for $\Delta = [2, 4, 6, 8, 10, 20, 30, 40, 50]$ milliseconds. The interaction timescale is of the order of 10 ms. In panel (b), the change in pitch angle of an electron interacting with an LAW for a single electron orbit as a function of time $\tau = \omega t$. The change in pitch angle, occurring within 10 ms, brings the electron in or near the loss cone, depending on the L-shell. Panel (c) shows the properties of the cold plasma dispersion relation as a function of propagation angle θ and wave frequency $\nu = \omega/\Omega_0$. Contours are drawn, starting from the bottom right corner, for refractive indices $N = c/v_\Phi = [10, 12, 14, 16, 18, 20, 25, 30, 35, 40]$.

Consequently, electrons trapped in the electrostatic field of the sub-element do not visit neighboring sub-elements for $\tau < 20$ ms. Following the breaking of trapping at higher latitude, the energy is on average conserved with the orbit well-described by adiabatic motion, making the remaining spatial structures unnecessary for our analysis. Examples of trapped electron orbits satisfying these conditions can be found in Artemyev et al. (2012) and Osmane & Hamza (2014).[6] If we were to quantify the energy gain and pitch-angle scattering for several bounce periods and several interactions with LAWs, we would need to take into account a more realistic wave model. Two additional effects can also alter our results. The first one is that the LAWs loose coherency at higher latitude (i.e., $\lambda > 25°$; Tsurutani et al. 2013). This loss of coherency will reduce the energy gain and pitch-angle scattering (Artemyev et al. 2012). A second effect is that waves with strongly oblique waves leave the initial field line after a time proportional to the transverse scale of the LAWs over the phase-speed. Transverse scales for LAWs are typically of 500 km and have a phase-speed of the order of 10^4 km s^{-1}. Hence, the available time for interaction is of the order of 50 ms, i.e., greater than the interaction timescale of 1–10 ms. Our study is therefore constrained to single interactions of electrons with LAWs in the equatorial plane. This approach allows us to approximate effects taking place on longer timescales, such as wave dispersion and self-consistent effects leading to the damping of the wave, as negligible (Yoon 2011). Future studies will examine the net effects of multiple interactions, loss of coherency at higher latitude, and the evolving size of the wave packet.

3.2. Particle and Energy Precipitation Fluxes

Once the orbits are computed, we build a map in pitch angle α and energy $E = m_e \gamma c^2$, denoted as $W(\alpha, E)$. The map is sampled uniformly with pitch angles $\alpha \in [7°, 20°]$ spread by an increment $\delta\alpha = 1°$ and Lorentz factor $\gamma \in [1.1, 2]$ spread by increment $\delta\gamma = 0.1$. Hence, we cover electrons with kinetic energies $(\gamma - 1)m_e c^2$ between 51 and 511 keV and energies E between 511 keV and 102 MeV with an initially empty loss cone. Additionally, we solve the orbits for a single wave phase. This choice is motivated by the study of the effect of the wave phase for trapped electrons by Osmane & Hamza (2014).[7] The map, or weight function, $W(\alpha, E)$ is given a value of one when a particle is pitch-angle scattered into the loss cone and zero when not. Following previous models of electron precipitation in the radiation belts (Lauben et al. 2001; Bortnik et al. 2006), we model the particle spectral density as $\psi(\alpha, E) = \psi_0 \frac{E_0^\eta}{E^\eta} q(\alpha)$, for the free parameters (ψ_0, E_0, η) set as $\psi_0 = 100$ electrons keV^{-1} cm^{-2} s^{-2}, $E_0 = 51.3$ keV and $\eta = 1$, where we have defined the function $q(\alpha) = \pi \sin(2\alpha)/\sin^2(\alpha_{\rm lc})$. Once the map $W(\alpha, E)$ from the particle orbits has been constructed, we can compute the particle fluxes as $N = \int_{\alpha_c}^{\pi/2} \int_{511\ \rm keV}^{1.02\ \rm MeV} \psi(\alpha, E) W(\alpha, E) d\alpha dE$ and the net energy fluxes $Q = \int_{\alpha_c}^{\pi/2} \int_{511\ \rm keV}^{1.02\ \rm MeV} E\psi(\alpha, E) W(\alpha, E) d\alpha dE$ accordingly. We note that the integration is computed for electrons initially outside of the loss cone (i.e., with pitch angles outside the loss cone $\alpha > \alpha_{\rm lc}$ at $t = 0$), such that particle and energy fluxes denote the precipitation contribution caused by LAWs solely.

4. RESULTS

4.1. Pitch Angle and Energy Precipitation Maps

Figure 2 shows examples of pitch-angle kinetic energy maps for electrons interacting with an LAW. It is from these maps that we construct the estimates of energy Q and particle N fluxes. The wave parameters are chosen as $\delta_1 = 0.05$, $\nu = 0.1$, and $n = 3$, for illustrative purposes. The six maps are plotted for varying propagation angles θ_{kB}. Red squares denote initial

[6] For instance, see the left panel of Figure 8 in Osmane & Hamza (2014).

[7] The effect of the wave phase has been investigated by Osmane & Hamza (2014). Numerical orbits were computed to determine the role of the wave phase on the Landau trapping. The overall conclusion was that the wave phase did not have an impact on the energization of Landau trapped electrons (though it does on electrons that are not Landau trapped) on timescales studied herein (i.e., of the order of 20 ms). For longer timescales the wave phase could determine whether the orbit would be trapped or quasi-trapped.

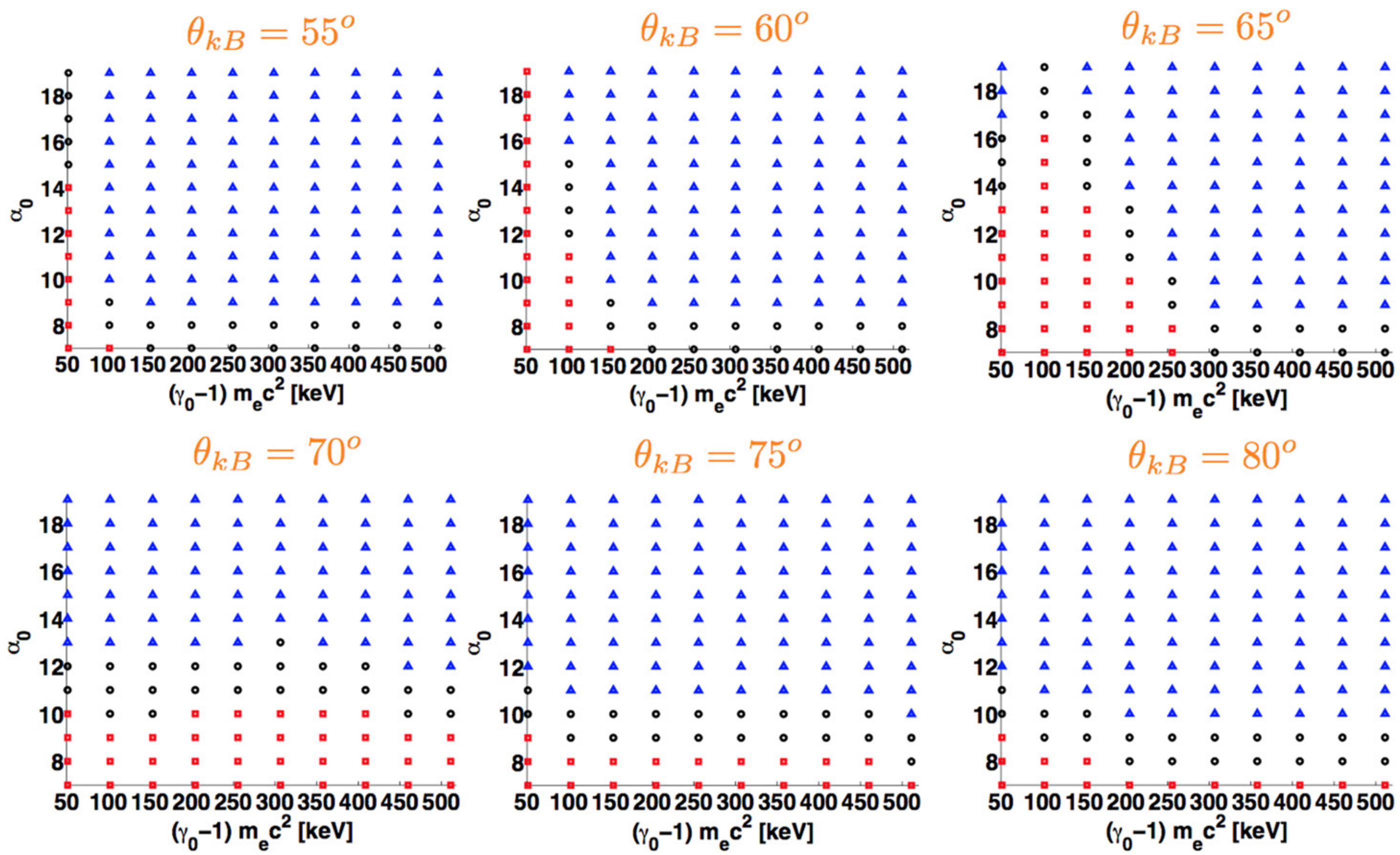

Figure 2. Pitch-angle (α) Kinetic energy $(\gamma_0 - 1)m_e c^2$ maps for electrons interacting with an LAW with $\delta_1 = 0.05$, $\nu = 0.1$, and $n = 3$. The six maps are plotted for varying propagation angles. Red squares denote initial pitch angles and kinetic energies of electrons scattered into the loss cone ($\alpha_{\rm lc} < 6.4$). Black circles denote initial electrons brought to the loss-cone boundary ($6.4 < \alpha < 7$). Blue triangles denote electrons that remain physically trapped in the magnetosphere. We note that as the propagation angle increases, the number of electrons scattered into the loss cone increases, reaching a maximum of $\theta = (65°\text{–}70°)$ and then decreasing for propagation angles of 75° and 80°. Additionally, we note that electrons with pitch angles of [12°–18°] can be precipitated after a single interaction.

pitch angles and kinetic energies of electrons scattered into the loss cone (here defined as $\alpha_{\rm lc} < 6.4$ for $L \simeq 6$). Black circles denote initial electrons brought close to the loss cone boundary (here defined as $6.4 < \alpha < 7$). Blue triangles denote electrons that should remain physically trapped in the magnetosphere after one interaction with an LAW. We note that as the propagation angle increases, the number of electrons scattered into the loss cone increases for the given values of n, δ_1, and ν, reaching a maximum for $\theta_{kB} = (65°\text{–}70°)$, and then decreasing for propagation angles of 75° and 80°. The decrease in the number of precipitating electrons above $\theta_{kB} \sim 70°$ can be explained by nonlinear trapping effects, as shown in previous studies (Osmane & Hamza 2012b, 2014). For a refractive index set as $n = 3$, Landau-resonant orbits cannot be physically trapped for propagation angles $\theta_{kb} > 71°$. Hence, this example demonstrates that increasing the parallel electric field or the propagation angle alone may not be sufficient to increase the efficiency of electron parallel energization and scattering. Trapping effects are, therefore, not only constrained by the wave amplitude, but also by the propagation angle and refractive index. Additionally, we note that electrons with kinetic energies <150 keV and with pitch angles of 12°–18°, can be efficiently scattered into the loss cone for propagation angles of 60°–65°. We note that even though the wave properties discussed above do not comply with the cold plasma dispersion relation, they correspond to properties of LAWs reported by Cattell et al. (2008), Kellogg et al. (2010, 2011) Breneman et al. (2011, 2012), and Wilson et al. 2011, and are indicative of the complex and efficient response to a single parameter change. In the following sections, we compute energy and particle precipitation fluxes for wave properties both within the cold plasma dispersion regime as well as outside.

4.1.1. *Effect of Wave Amplitude* $\delta_1 = \delta B/B_0$

Figure 3 demonstrates the impact of the wave amplitude on the precipitation fluxes as a function of propagation angle. The left panel denotes the energy flux Q as a function of propagation angles θ_{kB}, and parametrized for various values of wave amplitudes $\delta_1 = [0.009, 0.02, 0.04, 0.06, 0.08, 0.1]$. Embedded in the left panel is the logarithmic figure. The center panel denotes the particle fluxes N, and the right panel denotes the mean particle energy Q/N (units in eV) as a function of propagation angle. Embedded in the right panel is the ratio Q/N on a logarithmic scale. We note from these three panels, that as the amplitude of the wave increases, precipitation fluxes increase correspondingly. We observe a transition from hundreds of keV to MeV mean energy bursts occuring for $\theta_{kB} > 60°$. For $\theta_{kB} < 40°$, very few or no particles get scattered in the loss cone and the energy flux falls abruptly to zero. The peak in energy flux, particle flux, and mean energy values takes place for $\theta_{kB} \sim 70°$ because the maximum energization for the chosen refractive index $n = 3$ takes place in the vicinity of the Hopf–Hopf bifurcation for Landau-resonant electrons (Osmane

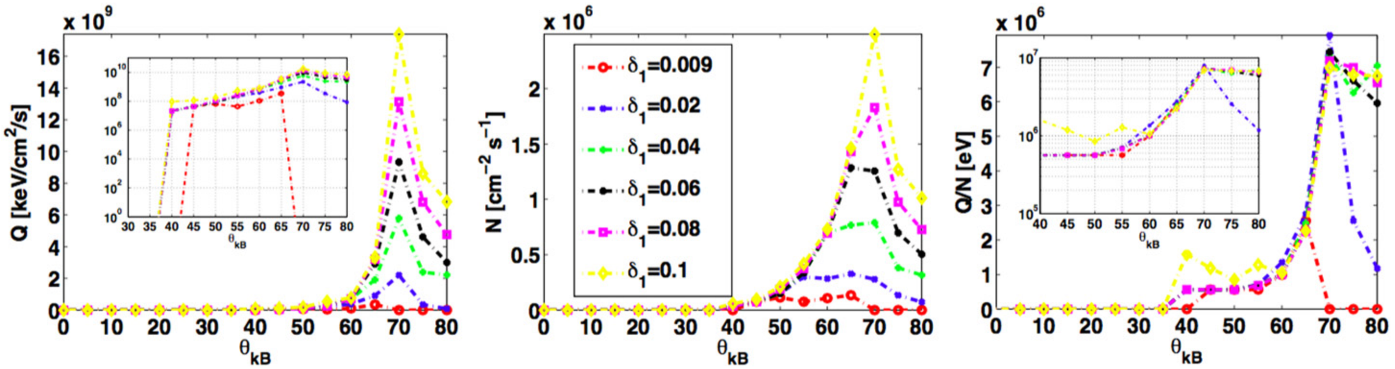

Figure 3. Energy flux Q (left panel), particle flux N (center panel), and mean energy Q/N as a function of propagation angle θ_{kB}, and for varying wave-amplitude δ_1. As the amplitude is increased, the energy flux increases. We note that the mean energy saturates at MeV levels for $\delta_1 \geqslant 0.02$ and that a transition from hundreds of keV electrons to MeV electrons occurs at $\theta > 60°$ and $\delta_1 \geqslant 0.02$.

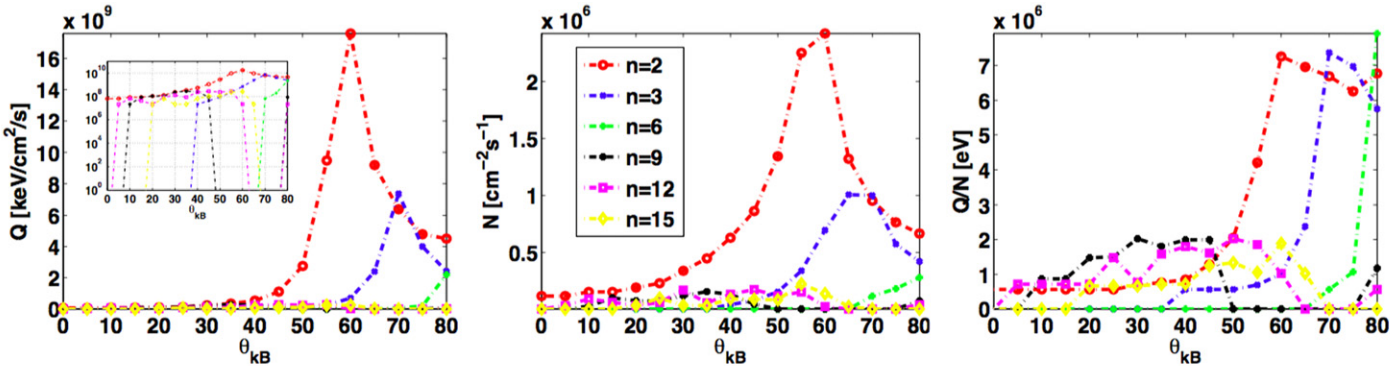

Figure 4. Energy flux Q (left panel), particle flux N (center panel), and mean energy Q/N as a function of phase-speeds. We note that the mean energy is typically of less than 1 MeV for parameters consistent with the cold plasma dispersion relation, but can reach MeV levels for phase-speeds $v_\Phi \geqslant c/9$ and large propagation angles $\theta_{kB} > 50$. Such values of the phase-speed and propagation angles are consistent with LAWs observed by Kellogg et al. (2010) and Wilson et al. (2011).

& Hamza 2012a). If we were to change the refractive index, this peak would shift to values given by $\tan(\theta_{kB}) = \sqrt{n^2 - 1}$. For instance, for $n = 2$, the peak would shift to $\theta_{kB} = 60°$. We also note that the mean particle energy saturates at MeV levels for $\delta_1 \geqslant 0.02$ and $\theta_{kB} > 60°$. This means that for wave amplitudes greater than 2% of the background field, there is no appreciable change in Q/N.

4.1.2. Effect of the Refractive Index $n = c/v_\Phi$

Figure 4 demonstrates the impact of the refractive index on the precipitation fluxes as a function of propagation angle. The left panel denotes the energy flux Q as a function of propogation angles θ_{kB}, and parametrized for various values of refractive indices $n = [2, 3, 6, 9, 12, 15]$. Embedded in the left panel, is the logarithmic plot for Q. The center panel denotes the particle fluxes N, and the right panel denotes the mean particle energy Q/N as a function of propagation angle. We note that the mean energy bursts Q/N are typically below the MeV level for parameters consistent with the cold plasma dispersion relation $n > 10$ and $\theta_{kB} < 30°$. We note that for LAWs to scatter particles into the loss cone through a single interaction to MeV levels, phase-speeds of $c > v_\Phi \geqslant c/9$ and large propagation angles ($\theta_{kB} \geqslant 50°$) are required. The enhancement in mean particle energy observed for $n > 9$ and resulting in values of $Q/N \sim 1$ MeV for smaller propagation angles is due to cyclotron-resonant (i.e., electrons for which $\omega - k_\parallel v_\parallel \sim \Omega_2/\gamma$) particles, rather than Landau-resonant electrons. However, we note that even though cyclotron resonance is a useful mechanism for generating microbursts, the trapping of Landau-resonant electrons is more efficient for large-amplitude whistlers capable of energizing a broader population caught in the potential well (Artemyev et al. 2014a). Consequently, we retain from this analysis that LAWs obeying the cold plasma dispersion can primarily generate keV microbursts. On the other hand, if large propagation angles associated with smaller refractive indices can be generated in the radiation belts, consistent with the LAW observations of Kellogg et al. (2010), they could produce relativistic microbursts in the MeV range through a single interaction.

4.2. Relationship between Quasi-stationary Electrostatic Structures and Microbursts

In the previous section, we have demonstrated that large-amplitude whistlers can result in the precipitation of electrons in the form of microbursts with energies ranging from keV to MeV energies. The impact of the energization and electron losses on the distribution function is schematically described in Figure 5. Following the interaction with the waves, Landau-resonant electrons are accelerated along the background magnetic field. The majority of the electrons do not enter the loss cone (with the boundaries between mirror trapped and untrapped electrons indicated by red lines), but a portion, quantified by the above analysis, do. As the electrons are entering regions of higher magnetic field, electrons outside of the loss cone bounce back, while those inside the loss cone are precipitated. The loss of electrons in the form of microbursts at

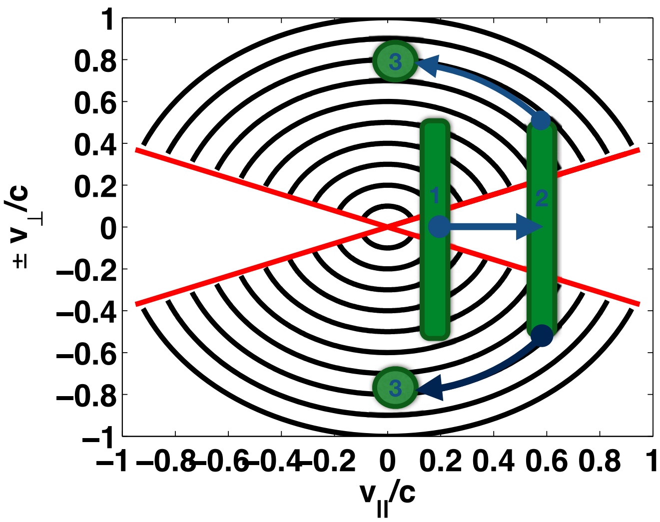

Figure 5. Schematic qualitatively describing how holes in the distribution are formed in one bounce period τ_b. The red boundaries indicate the loss cone, and the black lines indicate contours of constant energy in the $v_\parallel$–$v_\perp$ plane. Particles in the green area labeled as 1 are Landau resonant with the large-amplitude whistlers. They get accelerated parallel to the background field, with some entering the loss cone and others remaining outside the loss cone (label 2). Those who entered the loss cone will be precipitated, while those that are not, through conservation of the adiabatic invariant μ, bounce back at the mirror point (label 3). Consequently, at the mirror point, the distribution function experiences a hole, approximated by the analysis of microburst particle fluxes by $n_t/n_o \sim 0.1\%$–1%.

mirror points, therefore, results in holes of the electron distribution function around $v_\parallel = 0$. In this section, we demonstrate that electron kinetic structures discovered in the Earth's radiation belts by Mozer et al. (2013), Malaspina et al. (2014) can be generated as a consequence of microbursts and subsequent electron holes near mirror points ($v_\parallel = 0$).[8] We use microburst density depletions from the above analysis to quantify the size of holes and associated electric field amplitudes that can then be compared with data. We note that a self-consistent treatment of the problem describing large-amplitude whistler turbulence in an inhomogeneous magnetic field and populated by electrons ranging from tens of eV to a few MeV necessitates the artillery of numerical tools currently unavailable. By splitting the problem into three distinct parts (energization by oblique whistlers, microburst precipitation/hole formation, and electrostatic structure formation) the problem becomes analytically tractable and leads to predictions (particle/energy microbursts fluxes, amplitude of electrostatic structures, etc.) that can be compared with observations.

4.2.1. Reduced Quasi-stationary Vlasov Equation

In this section, we describe the wave–particle interaction of an electron of charge $-e$, mass m, and parallel momentum $p_\parallel$ in a slowly changing background magnetic field with the following Hamiltonian.

$$H = \frac{p_\parallel^2}{2\,m} + \mu B(s_\parallel) - e\Phi(s_\parallel, t), \tag{3}$$

where $s_\parallel$ is the position coordinate along the background magnetic field, $\mu = p_\perp^2/2mB$ is the conserved first adiabatic invariant, and Φ is the electric potential. We consider the dynamics of Landau trapped electrons resulting in vortex structures inside the distribution function, thus neglecting cyclotron resonances is justified. Hamilton's equations are given for this instance by $\dot{p}_\parallel = -\mu\partial B(s_\parallel)/\partial s_\parallel + \partial\Phi(s_\parallel, t)/\partial s_\parallel$ and $\dot{s}_\parallel = p_\parallel/m$. Assuming that phase-space density is conserved[9], that is, we are looking for electrostatic structures taking place on timescales of $\omega_{\rm pe}^{-1} \sim 10^{-4}$ s less than the bounce frequency (typically 0.1–1 s for electrons with 100 s of keV at $L > 5$) for which losses become important, we can write the Vlasov equation for the characteristics derived from the above Hamiltonian[10] in the following form.

$$\frac{\partial f}{\partial t} + v_\parallel\frac{\partial f}{\partial s_\parallel} + \left[-\frac{\mu}{m}\frac{\partial B}{\partial s_\parallel} + \frac{e}{m}\frac{\partial\Phi}{\partial s_\parallel}\right]\frac{\partial f}{\partial v_\parallel} = 0. \tag{4}$$

We then proceed by normalizing time with the plasma frequency $\omega_{\rm pe} = \sqrt{4\pi n_0 e^2/m}$, spatial scales with the Debye length $\lambda_{\rm D} = \sqrt{T_{\rm e}/4\pi n_0 e^2}$, and potential by the electron temperature in energy units $T_{\rm e}$. The normalized Vlasov equations can then be written for the normalized potential $\Psi = e\Phi/T_{\rm e} - \mu B/T_{\rm e}$ in a simplified form as

$$\frac{\partial f}{\partial \tau} + v\frac{\partial f}{\partial s} + \frac{\partial\Psi}{\partial s}\frac{\partial f}{\partial v} = 0. \tag{5}$$

We now now seek quasi-stationary solutions for the Vlasov equation for a background magnetic field of the form $B = B_0\cos(k_b s)$ in which the normalized wave vector $k_b = \sqrt{9}\,\lambda_D/R_{\rm E}L$ is written in terms of the Earth's radius $R_{\rm E} \sim 6300$ km s^{-1} and the L-shell L. A Galilean transformation to a frame of reference with constant speed $v_\Phi/v_{\rm the}$ yields a stationary electrostatic potential $\Phi(s, t) \rightarrow \Phi(s')$ but a time dependence in the magnetic field is introduced: $B(s) \rightarrow B(s', \tau)$. Following this transformation, we can write the normalized potential in terms of a stationary component Ψ_0 and a slowly time varying component $\Psi_1 \sim \epsilon(\tau)\Psi_0$ with

[8] There are infinite numbers of mirror points, a function of the equatorial pitch angle. We use the following expression to estimate the latitude of the mirror point. $\sin^2(\alpha_{\rm eq}) = \frac{B_{\rm eq}}{B_M} = \frac{\cos^6(\theta_M)}{\sqrt{1\ +\ 3\sin^2\theta_M}}$. The average pitch-angle scattering for wave amplitudes $0.09 \leqslant \delta_1 \leqslant 0.1$ is of the order of 1°. Consequently, the bulk of the precipitation will take place for particles with equatorial pitch angles between 6° and 7° and the mirror point with the deepest hole will be located at 57°.4 latitude ±1°.2. However, other holes formed at other magnetic mirror points can also result in double layers and solitary electron hole generation. Though beyond the scope of the paper, this effect could result in a train of nonlinear structures, similar to the one described by Mozer et al. (2013).

[9] We seek quasi-stationary (i.e., stationary for timescales of the order of a bounce period) electrostatic structure solutions arising at the mirror point following electron losses in the form of microbursts, i.e., when phase-space density is approximately conserved for another bounce motion. However, we can include a collision term denoting precipitation $\left(\frac{\partial f}{\partial t}\right)_c \sim 4\pi R_{\rm loss}\tau_{\rm b}^{-1} f$ where $4\pi R_{\rm loss}$ is the solid angle in velocity space of the loss cone, and $\tau_{\rm b}$ is the bounce frequency. Following the perturbation analysis defined below and the density depletion obtained from the previous section, indicating that only a fraction of electrons with $n_t/n_0 \sim 0.1\%$–1% are precipitated, the collision term is shown to always be smaller for microbursts than the perturbation term of the order $\epsilon \sim \lambda_\parallel R_{\rm E}^{-1}\omega_{\rm pe}\tau_{\rm b} \gg R_{\rm loss}\omega_{\rm pe}^{-1}\tau_{\rm b}^{-1} \sim 10^{-5}$. Hence, the following analysis is based on the initial existence of a hole in the distribution, but once the hole is formed, as a result of microburst events, additional precipitation does not alter the background distribution for timescales $T \ll \tau_{\rm b}$.

[10] The Hamiltonian in Equation (1) can be obtained by averaging the full Hamiltonian over the gyro-rotation (Cary & Brizard 2009).

$\epsilon = \frac{k_b \omega \tau}{k_\parallel}$:

$$\Psi = \Psi_0(s') + \Psi_1(s', \tau) = \frac{e\Phi_0(s')}{T_e} - \frac{\mu B_0}{T_e}\cos(k_b s') + \frac{k_b\omega\tau}{k_\parallel}\frac{\mu B_0}{T_e}\sin(k_b s') + \vartheta^2\left(\frac{k_b\omega\tau}{k_\parallel}\right), \tag{6}$$

where the term $\vartheta^2(\epsilon)$ indicates terms of the order of two and larger. Rewriting the Vlasov equation in terms of the new variables (s', v') to zeroth order in the small parameter $k_b v_\Phi \tau \sim \lambda_\parallel \omega t / L R_E \ll 1$, we find the following stationary equation.

$$v\frac{\partial f_0}{\partial s} + \frac{\partial \Psi_0}{\partial s}\frac{\partial f_0}{\partial v} = 0 \tag{7}$$

for $f_0 = f_0(s, v)$ and $\Psi_0 = \Psi_0(s)$ where the primes have been eliminated. The solution for the distribution function f_0 is correct for timescales $t \ll 10$ s, assuming the phase-speed of the electrostatic structure is of the order of 1–10 times the thermal electron speed. Such a timescale is of the order of a few bounce periods and is much larger than the typical kinetic electron scales $\tau_e \sim \Omega_{ce}^{-1}$ in the radiation belts. Hence, if we can find solutions to Equation (7) and the Poisson equation, with growth rates much larger than the bounce frequency, we can demonstrate that quasi-stationary electrostatic solutions can be generated self-consistently in the radiation belts. Since trapping in an electrostatic structure takes place on timescales comparable with the associated wave frequency, typically several orders of magnitude larger than the bounce frequency, a reduced description of the electron plasma is therefore possible.

4.3. *Electron Solitary Holes and Double Layer Solutions*

Equation (7) in association with Poisson's equation for Maxwellian ions has been formally derived by Kim (1983). The solution for the distribution of electrons can be rewritten as $f_0(E, \sigma) = 1/\sqrt{2\pi}$ $[\exp(-1/2(\sigma\sqrt{E} - v_d)^2 \Theta(E) + \exp(-1/2(\sigma\beta E - v_d^2)\Theta(-E)]$ where $\Theta(E)$ is the Heaviside function, $v_d = v_\Phi / v_{the}$, $E = v^2/2 - 2\Psi$, and σ is the sign of the normalized energy E. Following the recipe of Kim (1983), one can use Poisson's equation to derive an equation for Φ. In the limit $k_b s \ll 1$, $\partial^2\Psi/\partial s^2 \cong \partial^2\Phi/\partial s^2$, one can write Poisson's equation in the small amplitude limit (i.e., $\lambda_\parallel^2 / L^2 R_E^2 \ll \Phi / T_{\perp e} \ll 1$) in the form:

$$\frac{\partial^2\Phi}{\partial s^2} = A\Phi + B\Phi^{3/2} + C\Phi^2 + \vartheta^{5/2}(\Phi) \tag{8}$$

where the coefficients are defined by $A = T_e/T_i - Z'(v_d/\sqrt{2})$, $B = \frac{4e^{-v_d^2/2}}{3\sqrt{\pi}}(v_d^2 - \beta - 1)$, and $C = \frac{1}{2}e^{-v_d^2/2}(1 - T_e^2/T_i^2 e^{-v_d^2/2} + \frac{3e^{-v_d^2/2}}{4E^2})$, in which the parameter β (not to be confused with the kinetic to magnetic pressure of the plasma) controls the amount of trapped particles, and the function $Z'(v_d/\sqrt{2})$ represents the real part of the derivative of the complex dispersion function. The solution is found by imposing charge neutrality for $s = \pm\infty$ and by requiring that the electric field is zero outside of the electrostatic structure $\Phi = (0, \Phi_{max})$. Solutions for the quasi-stationary Vlasov–Poisson system results in two different types of solutions. The first solution, neglecting terms of the order of $\Phi^{3/2}$ and higher, consist in electron solitary holes written as

$$\Phi_{SEH} = 225\pi\left(\frac{\kappa^2 e^{\frac{v_d}{\sqrt{2}}}}{v_d^2 + \beta - 1}\right)^2 \cosh^{-4}(\kappa s) \tag{9}$$

for parameters $\kappa = \pm 1/4\sqrt{T_e/T_i - Z'(v_d)/2}$, $\beta - 1 = v_d^2 - 30\sqrt{\pi}e^{v_d^2/2}\kappa / \sqrt{\Phi_{max}}$, and $\Phi_{max}^{-1/2} = (e^{-v_d^2/2} - T_e/T_i - 3/2v_d^2)/48\kappa^2$. Similarly, if one keeps a term of the order of $\Phi^{3/2}$, one can find an electron double layer solution written in terms of the above parameters as

$$\Phi_{DL} = \left(\frac{15\sqrt{\pi}\kappa^2 e^{v_d^2/2}}{v_d^2 + \beta - 1}\right)^2 (1 + \tanh(\kappa s))^2. \tag{10}$$

We can now make use of the density of electrons lost in the form of microbursts as a means to obtain an estimate of β. Once the parameter β is obtained, one can find an associated value for $v_d = v_\phi / v_{the}$ and then the range of amplitudes for the electron solitary holes and double layers. Figure 6(a) shows the change in the distribution function for various values of β. Figure 6(b) shows the dependence of electrostatic structures as a function of the parameter β.

4.3.1. *Effect of Temperature Anisotropy T_e/T_i on the Instability*

The instability criterion for the generation of both double layers and electron solitary holes is highly dependent on the temperature anisotropy τ. The electron distribution in the radiation belts observed in association with double layers have been reported to have thermal speeds of the order of 25 eV by Mozer et al. (2013). In a statistical study of LAWs by Wilson et al. (2011), one could deduce from the LAW associated distribution functions thermal spread of the order of 20–650 eV. The ion distribution function on the other hand were shown by Spjeldvik (1997) to have a thermal spread of a few keV to hundreds of keV, depending on the L-shell. Additionally, ions injected into the radiation belts have thermal speeds of the order of 3 keV (Onsager et al. 1991). In Figure 7, we have plotted the parameter space consistent with the generation of double layer and electron solitary hole solutions. The instability can be generated for temperature anisotropies $T_e/T_i < 30\%$, for a trapping parameter of $\beta < -0.70$ and electron drift energy, in the frame of the stationary ions and normalized by the electron thermal energy, of $E_d > 0.9$.[11] These values overlap with the values inferred from radiation belt measurements. Taking a ratio of the electron to ion temperature $T_e/T_i \sim 25/1000 \ll 1$, we find that for electron holes of the order of 0.1%–10%, electrostatic structures with electric fields as large as 1 mV m^{-1} can be generated for various hole sizes.

4.3.2. *Stability of Nonlinear Electrostatic Structures: Necessity for $\delta f < 0$ Near Mirror Points*

The self-consistent potential due to an electron phase-space hole in its rest frame can be written in non-normalized form as

[11] See also Kim (1983) in the text under Equation (7), where he notes that the temperature anisotropy is $\tau < 0.285 + \epsilon$ for a small parameter ϵ.

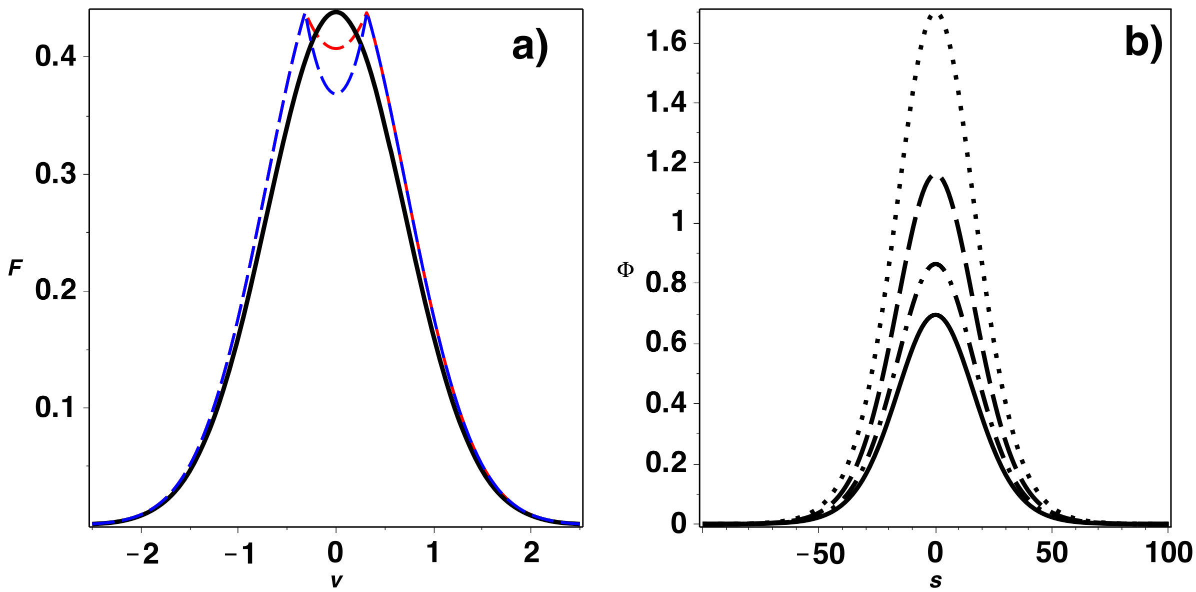

Figure 6. Distribution function of the parallel velocity ($v_\parallel = \boldsymbol{v} \cdot \boldsymbol{B}_0$) without electron hole ($\Phi = 0$) in black, and with electron holes ($\Phi_0 = 0.1$, $\beta = -0.74$) in red and ($\Phi_0 = 0.1$, $\beta = -1.74$) in blue, respectively, corresponding to density holes of the order of 1% and 5%. In panel (b), the normalized potential as a function of the normalized spatial variable for different values of the parameter $\beta = [-1.24, -1.34, -1.54, -1.74]$ corresponding to the solid, dashed–dotted, dashed, and dotted lines, respectively. The parameter β controls the amount of precipitated particles. As β increases, the amplitude of the electrostatic structure is constrained to smaller values.

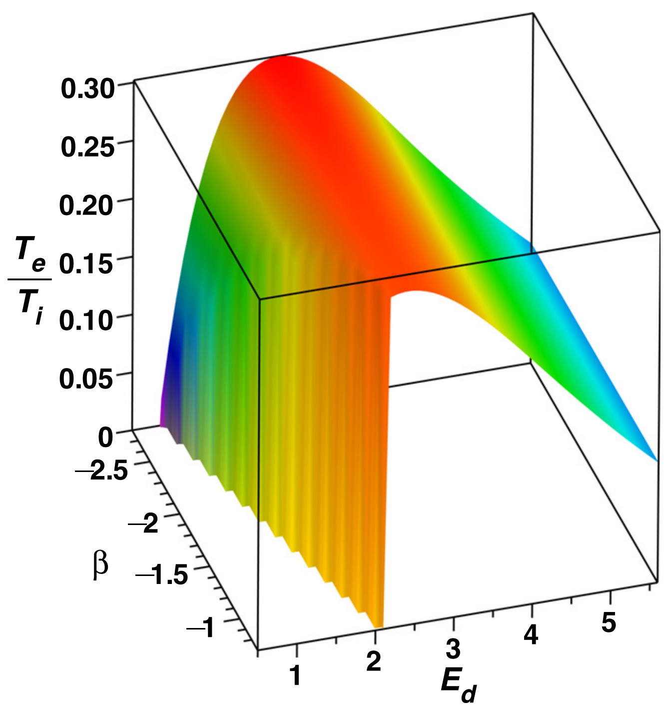

Figure 7. Parameter space for the validity of the double layer and electron solitary holes solution. The instability can be generated for temperature anisotropies $T_e/T_i < 30\%$, for a trapping parameter $\beta < -0.70$ and electron drift energy, in the frame of the stationary ions and normalized by the electron thermal energy, $E_d > 0.9$.

(Dupree 1982)

$$-\frac{\partial^2 \Phi}{\partial s_\parallel^2} + \Lambda^{-2}\Phi = 4\pi e \int_{-\Delta v_\parallel/2}^{\Delta v_\parallel/2} \delta f dv_\parallel, \qquad (11)$$

where δf is the change in the distribution function in the vicinity of the mirror point $v_\parallel = 0$, i.e., $\delta f = 0$ for $|v| > \Delta v_\parallel/2$ and $\delta f = f_0(E, \sigma; \beta = 0) - f_0(E, \sigma; \beta \neq 0)$ for $|v| \leqslant \Delta v_\parallel/2$. The right-hand side represents the charge density of the hole situated at $v_\parallel = \pm\Delta v_\parallel/2$ and Λ is the plasma shielding length function of the dielectric function ε and written as $1/\Lambda^2 = k^2[\Re\varepsilon(k, ku) - 1]$. As pointed out by Dupree (1982), the self-interaction term due to the presence of the phase-space hole can lead to self-bound electrostatic structures. The left-hand side is proportional to $k^2\varepsilon\Phi$, and it follows that since $e\Phi < 0$, $\delta f/\varepsilon < 0$. Hence, if $\varepsilon > 0$, that is for holes taking place at $v_\parallel \sim 0$ near the mirror point, a bound state requires $\delta f < 0$.[12] Hence the negative fluctuations tend to self-trap, whereas the positive fluctuations are unstable. In the following sub-section, we derive a relationship between phase-space density hole depth $\delta f/f$ and size $\Delta v_\parallel$.

4.3.3. Constraint on Phase-space Hole Depth δf and Width $\Delta v_\parallel$

From Equation (11), we can derive a relationship between the width of the electron hole and its depth quantified by δf, which is necessary for the existence of stable nonlinear electronic structures. We know from the microburst analysis that the dimension of the hole along the field line $\Delta s_\parallel$ scales as $LR_E\delta\theta \sim 5 * 6300$ km $* 1^\circ\!.2 = 550$ km since the bulk of the precipitated electron have equatorial pitch angles between 6° and 7°. This dimension is much larger than the shielding length Λ, which itself is proportional in magnitude to the Debye length λ_{De} for very small holes. Consequently, $1/\Delta s_\parallel^2 \ll \Lambda^{-2}$, and we can approximate Equation (11) as $\Lambda^{-2}\Phi \simeq 4\pi e\delta f\Delta v_\parallel$. This expression can be written in terms of the normalized

[12] We note that bumps or beams with similar densities in the distribution functions due to Landau trapped electrons with $v \gg v_{th}$ could also lead to stable nonlinear structures on similar timescales. We here take the perspective of a hole near a mirror point to simplify the analytical treatment.

coordinates as

$$\frac{1}{\Lambda^2}\frac{e\phi}{T_e} = \frac{4\pi e^2}{T_e}\frac{\delta f}{f(0)}\frac{\Delta v_\parallel}{v_{th}} f(0) v_{th} \simeq \frac{1}{\lambda_D^2}\frac{\delta f}{f(0)}\frac{\Delta v_\parallel}{v_{th}} \tag{12}$$

where $f(0)$ stands for the maximum value of the distribution at the mirror point and $n_0 \sim f_0 v_{th}$. In order for seed fluctuations of nonlinear electrostatic structures to grow and be stable, the following condition must be respected:

$$\left|\frac{\delta f}{f(0)}\frac{\Delta v_\parallel}{v_{th}}\right| > \left|\frac{\lambda_D^2}{\Lambda^2}\frac{e\phi}{T_e}\right| \simeq 10^{-2}\text{–}10^{-3}, \tag{13}$$

where we used values derived from the model of Kim (1983) of $e\Phi/T_e \sim 0.1 - 0.01$ and $\lambda_D/\Lambda \sim 1/4$ corresponding to seed electric fields of $E \sim 1\,\mathrm{mV\,m^{-1}}$. This constraint indicates that the larger the nonlinear electrostatic structures, the larger the hole depth and/or width needs to be. With the numerator being proportional to the density of precipitated electrons n_t, and the denominator to the background density in the vicinity of the mirror point, we estimate that the precipitated electron ratio n_t/n_0 of the order of 0.1%–1% can result in stable seeds for nonlinear structures.

4.3.4. Summary of Results on Nonlinear Structures

Despite the approximations made (reducing the problem to a one-dimensional, electrostatic equation), we have shown that in the classical limit and for timescales much smaller than several bounce periods, the precipitation of electrons in the form of microbursts can result in stable electrostatic structures one order of magnitude below typically observed amplitudes (i.e., we theoretically obtain $E \sim 1\,\mathrm{mV\,m^{-1}}$ whereas observations show $E \sim 10$–$20\,\mathrm{mV\,m^{-1}}$). These results are also consistent with the numerical study of Drake et al. (2015) showing that electron bursts resulting from the interaction with LAWs can lead to electrostatic structures. The parameter regime of the above model requires $T_e/T_i < 0.30$ and is consistent with the observations of precipitation of keV electrons with small density holes on the order of $n_t/n_0 \sim 0.1\%$–1%. Landau-resonant energetic electrons in the radiation belts only count for about 1% of the cold electron population. Whistlers with very large-amplitude $\delta_1 > 0.04$ and strong obliquity $\theta_{kB} > 50°$ are, therefore, more likely to generate microbursts and produce seed fluctuations for stable nonlinear electrostatic structures. Finally, we would like to stress that the reduction the wave–particle interaction to a one-dimensional problem is only valid for electron time scales ω_{pe}^{-1}. The wave–particle interactions and the stability and generation of nonlinear structures on longer timescales will require a study incorporating additional spatial dimensions and more realistic fields.

5. CONCLUSION

Using a dynamical-system approach, we have investigated the efficiency of LAWs for causing microburst precipitation by modeling the microburst energy and particle fluxes produced as a result of nonlinear wave–particle interactions. We have found that microbursts of keV and MeV energies are generated for a wide range of propagation angles and amplitudes. However, because of the constraint on the refractive index and wave propagation, whistlers derived from the cold plasma dispersion relation cannot cause relativistic MeV microbursts after one single interaction. These results, therefore, indicate that relativistic microbursts, such as those observed by SAMPEX/HILT from low-Earth orbit (Blake et al. 1996; Kersten et al. 2011) are generated either by multiple interactions of electrons with whistlers in the cold plasma regime or by the single interaction of electrons with LAWs outside of the cold plasma regime.

Additionally, we have shown that as a consequence of microbursts and the resulting phase-hole in the velocity distribution function, electrostatic structures consistent in scales (of the order the Debye length) and amplitudes (of the order of $1\,\mathrm{mV\,m^{-1}}$) to nonlinear structures observed in the radiation belts (Mozer et al. 2013; Malaspina et al. 2014) could be generated on timescales much smaller than several electron bounce periods for precipitated densities of the order of 0.1% of the background electron density, i.e., if energetic electrons form 1% of the radiation belts, we estimate that 1/10 of energetic particles precipitated could lead to the generation of nonlinear electrostatic structures. It should be pointed out that holes in the distribution function of electrons, as a result of trapping by LAWs and/or microburst precipitations, are not the only means through which double layers and electron solitary holes can be generated. In a recent study, Agapitov et al. (2015) showed that nonlinear electronic structures could be generated as a result of a parametric decay of whistler waves. Similarly to our study, they find that the decay instability possesses a characteristic time smaller than 1 s, consistent with observations.

Finally, our results point to the inherent relationship between nonlinear electronic structures in the Earth's radiation belts and their role in the acceleration and precipitation of electrons on kinetic timescales. Large-amplitude whistlers contribute to the acceleration and precipitation of electrons. Electron trapping and precipitation of electrons allows formation of electrostatic structures, which were shown to accelerate particles to keV levels (Artemyev et al. 2014b; Osmane & Pulkkinen 2014) and therefore feed further energization by whistlers. The mechanisms described here and in previous theoretical studies (Artemyev et al. 2012, 2014a; Osmane & Hamza 2012b, 2014), therefore, provide a self-contained cycle upon which radiation belts can continuously create a fresh population of keV electrons. keV electrons with smaller pitch angles will eventually precipitate, and cause the generation of electrostatic structures leading to a newly formed keV-energy electron population. In a ten-year statistical study of radiation belts, Artemyev et al. (2015) demonstrated that strongly oblique whistlers ($\theta > 60°$) with small magnetic components, but strong electric fields, have been systematically under-sampled and, consequently, their impact in regulating the belts underestimated. The implication of our results, in conjunction with observations by Mozer et al. (2013, 2014), Malaspina et al. (2014), Agapitov et al. (2015), and Artemyev et al. (2015) is that nonlinear electronic structures, i.e., large-amplitude oblique whistlers and double layers, might have a central role in regulating the radiation belts on kinetic timescales. Even though the above mechanisms have yet to be shown to regulate the dynamics of radiation's belts on long timescales, they have the potential to dominate the depletion and enhancement of the keV radiation belts' electrons over other mechanisms due to the very small timescale involved. Future studies will improve upon the discretized microburst model and dynamical system described herein to extend our results to longer timescales (e.g., comparable to or greater than the bounce period).

This work was supported by the Academy of Finland grant #267073/2013. L.B. acknowledges the JHU/APL contract 922613 (RBSP-EFW). The authors would like to thank the reviewer for insightful comments that significantly improved the manuscript.

REFERENCES

Agapitov, O. V., Artemyev, A. V., Mourenas, D., et al. 2014, JGR, 119, 1606
Agapitov, O. V., Krasnoselskikh, V. V., Mozer, F. S., Artemyev, A. V., & Volokitin, A. S. 2015, GeoRL, 42, 3715
Anderson, K. A., & Milton, D. 1964, JGR, 69, 4457
Artemyev, A. V., Krasnoselskikh, V. V., Agapitov, O. V., Mourenas, D., & Rolland, G. 2012, PhPl, 19, 122
Artemyev, A. V., Vasiliev, A. A., Mourenas, D., et al. 2014a, GeoRL, 41, 5727
Artemyev, A. V., Vasiliev, A. A., Mourenas, D., Agapitov, O. V., & Krasnoselskikh, V. V. 2014b, PhPl, 21, 903
Artemyev, A. V., Agapitov, O. V., Mozer, F. S., & Krasnoselskikh, V. V. 2014c, GeoRL, 41, 5734
Artemyev, A. V., Agapitov, O. V., Mourenas, D., Krasnoselskikh, V. V., & Mozer, F. S. 2015, Natur, 6, 7143
Blake, J. B., Looper, M. D., Baker, D. N., et al. 1996, AdSpR, 18, 171
Bortnik, J., Inan, U. S., & Bell, T. F. 2006, JGR, 111, 2204
Bortnik, J., Thorne, R. M., & Inan, U. S. 2008, GeoRL, 35, L21102
Breneman, A., Cattell, C., Wygant, J., et al. 2011, JGR, 116, A06310
Breneman, A., Cattell, C., Wygant, J., et al. 2012, JGR, 117, A04317
Cary, J. R. A. J., & Brizard, A. J. 2009, RvMP, 81, 693
Cattell, C., Wygant, J. R., Goetz, K., et al. 2008, GeoRL, 35, L01105
Cattell, C., Breneman, A., Goetz, K., et al. 2012, in Dynamics of the Earth's Radiation Belts and Inner Magnetosphere, ed. D. Summers et al. (Washington, DC: AGU), 41
Chen, Y., Reeves, G., & Friedel, R. 2007, Natur, 3, 614
Cully, C. M., Bonnell, J. W., & Ergun, R. E. 2008, GeoRL, 35, L17S16
Diamond, P. H., Itoh, S.-I., & Itoh, K. 2010, Modern Plasma Physics: Physical Kinetics of Turbulent Plasmas (Cambridge: Cambridge Univ. Press)
Drake, J., Agapitov, O., & Mozer, F. 2015, GeoRL, 42, 2563
Dupree, T. H. 1982, PhFl, 25, 2
Green, J. M. Kivelson. 2004, JGR, 109, A03213
Hikishima, M., Omura, Y., & Summers, D. 2010, GeoRL, 37, L07103
Imhof, W. L., Voss, H. D., Mobilia, D. W., et al. 1992, JGR, 97, 829
Kellogg, P. J., Cattell, C. A., Goetz, K., Monson, S. J., & Wilson, L. B., III 2010, GeoRL, 37, L20106
Kellogg, P. J., Cattell, C. A., Goetz, K., Monson, S. J., & Wilson, L. B., III 2011, JGR, 116, A09224
Kersten, K., Cattell, C., Breneman, A., et al. 2011, GeoRL, 38, L08107
Kim, K. Y. 1983, PhLA, 97, 45
Lakhina, G. S., Tsurutani, B. T., Verkhoglyadova, O. P., & Pickett, J. S. 2010, JGR, 115, A00F15
Lauben, D. S., Inan, U. S., & Bell, T. F. 2001, JGR, 106, 745
Lorentzen, K., Blake, J., Inan, U., & Bortnik, J. 2001, JGR, 106, 6017
Malaspina, D. M., Andersson, L., Ergun, R. E., et al. 2014, GeoRL, 41, 5693
Mozer, F. S., Bale, S. D., Bonnell, J. W., et al. 2013, PhRvL, 111, 235002
Mozer, F. S., Agapitov, O. V., Krasnoselskikh, V. V., et al. 2014, PhRvL, 113, 035001
Nakamura, R., Baker, D. N., Blake, J. B., et al. 1995, GeoRL, 22, 1129
Onsager, T. G., Thomsen, M. F., Elphic, R. C., & Gosling, J. T. 1991, JGR, 96, 20999
Osmane, A., & Hamza, A. 2012a, PhRvE, 85, 5
Osmane, A., & Hamza, A. 2012b, PhPl, 19, 030702
Osmane, A., & Hamza, A. 2014, NPGeo, 21, 115
Osmane, A., & Pulkkinen, T. J. 2014, JGR, 119, 8243
Parks, G. K. 1978, JGG, 30, 327
Reeves, G. D., Spence, H. E., Henderson, M. G., et al. 2013, Sci, 341, 991
Santolik, O., Gurnett, D. A., Pickett, J. S., Parrot, M., & Cornilleau-Wehrlin, N. 2001, GeoRL, 31, 5693
Spjeldvik, W. K. 1997, JGR, 82, 2801
Summers, D., & Omura, Y. 2007, GeoRL, 34, L24205
Tao, X., & Bortnik, J. 2010, NPGeo, 17, 599
Thorne, R. M., Li, W., Ni, B., et al. 2013, Natur, 504, 411
Tsurutani, B. T., Lakhina, G. S., & Verkhoglyadova, O. P. 2013, JGR, 118, 2296
Wilson, L. B., III, Cattell, C. A., Kellogg, P. J., et al. 2011, GeoRL, 38, L17107
Woodroffe, J., & Streltsov, A. 2014, JCoPh, 276, 468
Yoon, P. H. 2011, GeoRL, 38, L12105
Yoon, P. H., Pandey, V. S., & Lee, D.-H. 2013, PhPl, 20, 112902
Yoon, P. H., Pandey, V. S., & Lee, D.-H. 2014, JGR, 119, 1851